ESTEEM Academic Journal
Vol. 19, March 2023, 54-67

Analysis of Flexible Silver-printed NFC Tag Antenna on Miniaturization and Bending Effect

Najwa Mohd Faudzi[1], Ahmad Rashidy Razali[2], Asrulnizam Abdul Manaf[3], Nurul Huda Abd Rahman[4], Ahmad Azlan Aziz[5], Amiruddin Ibrahim[6] and Aiza Mahyuni Mozi[7]
[1,2,6,7]*School of Electrical Engineering, Universiti Teknologi MARA, Cawangan Pulau Pinang, Pulau Pinang, Malaysia*
[3]*Collaborative Microelectronic Design Excellence Center, Universiti Sains Malaysia, Malaysia*
[4]*Antenna Research Centre, School of Electrical Engineering, College of Engineering, Universiti Teknologi MARA, Shah Alam, Selangor, Malaysia*
[5]*Universiti Teknologi Brunei, Brunei Darussalam*
**Corresponding author: [2]ahmad073@uitm.edu.my*

ARTICLE HISTORY

Received
27 January 2023

Accepted
15 March 2023

Available online
31 March 2023

ABSTRACT

Size and flexibility are the two main elements that must be considered in designing a near-field communication (NFC) tag antenna because they will determine the performance of the whole system. The previously designed NFC tag antenna, which is made of a rigid substrate such as FR-4, limited the application of the tag to only on a flat surface. The size of the tag antenna also needs to be optimised based on the application requirements since different sizes of the antenna will contribute to different electrical properties, including inductance and resistance. Therefore, this paper presents an analysis of a flexible printed tag antenna with different miniaturisation sizes and bending effects for NFC systems. The operating frequency of the proposed NFC tag antenna is 13.56 MHz, which is the same frequency as the NFC reader, allowing them to be coupled and to communicate with each other. Three sizes of silver printed tag antenna are presented, and the performance of the tag during bending is analyzed. Other tag antenna parameters and characteristics, including reflection coefficient, inductance, resistance, read range and output voltage, are also observed through simulation and accordingly measured. The results show that the Design 1 antenna has demonstrated the highest measured tag reading range of 3 cm, while the Design 2 antenna has shown good flexibility, withstanding bending at various angles and exhibiting a minimum reading range of 0.5 cm. Overall, the correlation between antenna size, flexibility and antenna performance has been determined and systematically validated.

Keywords: *flexible, miniaturization; Near Field Communication; tag; antenna*

1. INTRODUCTION

Near-field communication (NFC) is a technology that enables non-contact point-to-point data transmission and exchange between two devices over a short distance and has recently gained significant attention owing to its high security and easy operation method. Developed based on radio frequency identification (RFID), which operates at a high-frequency band (13.56 MHz) [1], NFC has features such as battery-less passive mode, wireless communication and fast, non-contact data transfer, making it a promising tool for physiological signal measurement. In NFC systems, the communication between the reader and the tag antennas is based on inductive coupling, where the energy required is generated by the magnetic field of the reader [2]. By placing the NFC-enabled device (e.g. smartphone, smart tablet or NFC reader) close to the NFC

p-ISSN 1675-7939; e-ISSN 2289-4934

tag antenna, the energy is harvested and powers up the chip together with other external electronic components, including microcontrollers and sensors. Depending on its power supply, the tag can operate in an active or passive mode.

Tag antenna plays a critical role in NFC systems because it is responsible for energy and data transfer [3]. The antenna design must be coil shaped to be inductively coupled with the reader and power up the chip [4]. The size of the loop coil is the most important aspect of antenna design, as the antenna Q factor, reading range and transfer efficiency are determined by the appropriate size of the loop coils [5-8]. However, the size of the antenna depends mostly on the application of the tag antenna itself. In some cases, the size of the antenna must be very small as proposed in [9], where the antenna needs to be attached to a small surface area like nails, teeth and so on. If the size of the antenna is not crucial, then the antenna can be designed as big as a credit card as proposed in [10] to get an optimum overall performance.

Other than antenna size, the flexibility of the tag antenna is also one of the major concerns in certain applications. Previously, most NFC tag antennas were fabricated on rigid substrates, such as FR-4 and PCB board, as proposed in [11-13]. However, these rigid substrates limit the application of the tag antenna to be attached to a flat surface structure. Several researchers have proposed NFC tag antenna on a flexible substrate for example paper, textile, polyethylene terephthalate (PET) and Kapton as listed in Table 1. In addition, the list presents the fabrication technique that has been used to fabricate the flexible NFC tag antenna. Screen printing offers simple patterning techniques, but the large quantity of materials required during the printing process will reduce the cost-efficiency. Meanwhile, inkjet printing offers several advantages for flexible antenna printing including fast printing, less material waste, controlled material deposition and compatible with different substrates [14]. Table 1 also lists some of the previous studies that have conducted bending tests. Nonetheless, there have been relatively fewer investigations that have specifically focused on assessing the impact of bending on the read range of the antenna.This study will analyze the characteristics of flexible silver-printed NFC tag antenna with different sizes and its bending effect when attached on different curvatures. Some parametric studies will also be conducted to determine the effect of varying the antenna parameters, including coil width, gap and number of turns, to the antenna resistance and inductance. The fabrication and measurement process will also be extensively discussed in this paper. The rest of the paper is organized as follows: Section II describes the antenna design structure, Section III explains the parametric studies, Section IV reports the results from the simulation and measurement and Section V summarizes the conclusions and recommendations for future work.

Table 1: NFC tag antenna with different flexible substrates and fabrication techniques

Author	Antenna Size (mm^2)	Flexible Substrate Material	Fabrication Technique	Bending Testing	Ref.
Zhang	46 x 32	PET	Screen printing	No	[15]
Leng	74 x 53	Paper	Screen printing	No	[16]
Ortego	80 x 50	Kapton Polymide	Inkjet printing	No	[17]
Scida	45 x 75	PET, Kapton, PEN, PC, PVC and paper	Laser ablation and robotic cutting plotter	Yes	[10]
Jiang	68 x 68	Textile	Embroidery	Yes	[18]
Maskey	70 x 40	Polymide	Roll-to-Roll Gravure printing	No	[3]

p-ISSN 1675-7939; e-ISSN 2289-4934

2. ANTENNA DESIGN STRUCTURE

Figure 1 (a)–(c) show the structure of the NFC tag antenna at different sizes, which was designed using CST Simulation software. The conductive ink used for the tag antenna design is silver ink with a conductivity and thickness of 6.3012×10^7 S/m and 0.01 mm, respectively. The silver ink was printed on a flexible PET substrate with the electrical permittivity ε_r of 3 and a thickness of 0.12 mm. PET substrate was chosen instead of other flexible substrates (e.g. paper and TPU) because of its low thermal shrinkage and better adhesion [15]. A discrete port was inserted in the antenna design, which indicates the NFC chip. The NFC chip used in the antenna design was an RF430FRL152HCRGER chip from Texas Instrument and has an internal capacitance C_{int} of 35 pF [19].

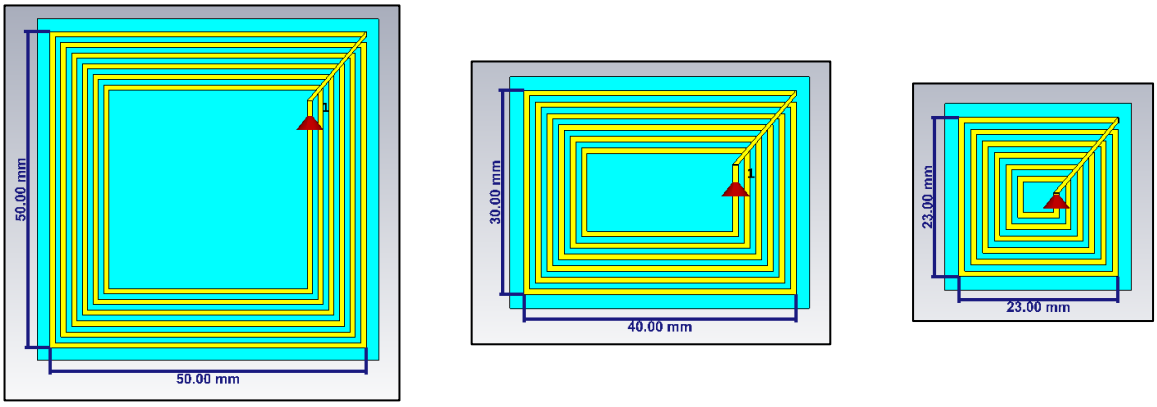

(a) (b) (c)

Figure 1: Antenna structure of (a) Design 1, (b) Design 2 and (c) Design 3

The dimensions and parameters for each antenna design are listed in Table 2. The miniaturization process has been achieved through the variation of the tunable capacitance, Ctun, which is connected in parallel to the internal capacitor of the chip as depicted in Figure 2 (a). With the increase of the tunable capacitance value as referred to Equation (1), the antenna inductance will be decreased to achieve impedance matching at 13.56 MHz, thus resulting to a smaller size of the tag antenna. Designs 2 and 3 were miniaturized from Design 1 at approximately 52 % and 79 %, respectively. The equivalent circuit of the tag antenna, tunable capacitor and NFC chip is depicted in Figure 2 (b). In the tag antenna equivalent circuit, the value of L_2 is specified by the number of turns, R_2 is specified by the diameter and length of antenna wire and C_p is specified by the distance between antenna wires and the number of turns [20].

Table 2: Antenna Parameters

Antenna Design	Design 1	Design 2	Design 3
Dimension (mm^2)	50 × 50	30 × 40	23 × 23
Conductor width, *w* (mm)	0.8	0.8	0.8
Gap between conductors, *g* (mm)	0.9	0.9	0.9
Number of turns, *n*	6	6	6

p-ISSN 1675-7939; e-ISSN 2289-4934

(a) (b)

Figure 2: (a) Matching circuit in CST Design Studio and (b) equivalent circuit of NFC tag

$$L_{ant} = \frac{1}{4\pi^2 f_{res}^2 \cdot (C_{int} + C_{tun} + C_p)} \quad (1)$$

3. PARAMETRIC STUDY

Several parametric studies were conducted for all antenna designs to determine the effect of varying the number of turns, the gap between the conductors and the width of the conductor to the antenna resistance (Ra) and antenna inductance (La).

3.1 Different Number of Turns, n

The number of turns in the coil antenna design is represented as the antenna inductance in the antenna equivalent circuit. Theoretically, inductance is higher in a coil than in a straight wire when the same material is used [21]. Figure 3 shows the effects of La and Ra when the number of turns is increased from 4 to 6. It shows that increasing the number of turns while maintaining the overall dimension will simultaneously increase the values of La and Ra. Design 1 showed a significant increment of La from 1.51 µH to 2.58 µH, with an increase of approximately 0.5 µH for each increment of turn number. On the other hand, Designs 2 and 3 showed only a slight increment of La from 0.82 µH to 1.26 µH and 0.39 µH to 0.48 µH, respectively. This is because the total coil length of Design 1 was longer compared to those of Designs 2 and 3, a condition that also contributes to the larger value of antenna inductance. The relationship between antenna inductance and the number of coils are supported by the following Equation (2).

$$L = \frac{N\mu HA}{I} \quad (2)$$

where N is the number of turns, μ is the permeability, H is the field strength, A is the surface area, and I is the current. As for its corresponding Ra variation, the Ra value for Designs 1 and 2 has shown increments, from approximately 0.9 Ω to 1.49 Ω and 0.58 to 0.89, respectively. Notably, the Ra for Design 3 showed an even smaller variation from 0.32 Ω to 0.46 Ω.

p-ISSN 1675-7939; e-ISSN 2289-4934

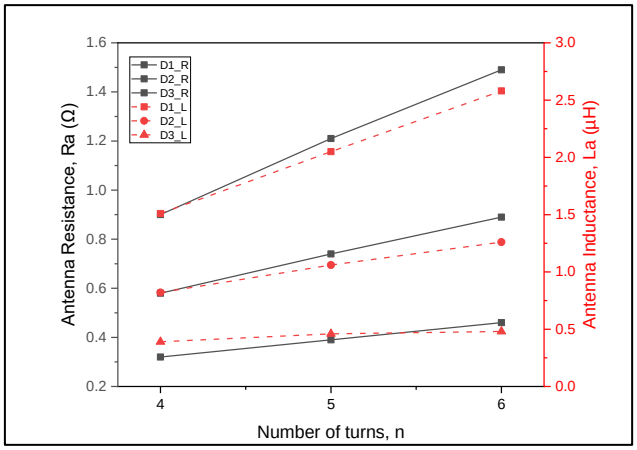

Figure 3: Ra and La with respect to the number of turns

3.2 Different Gap Between the Conductors, g

In the parametric study, the conductor gap (g) was varied from 0.7 mm to 0.9 mm while other parameters remained the same. As depicted in Figure 4 (a), increasing the gap between conductors simultaneously decreases the values of La and Ra. The effect of varying the conductor gap (g) for Design 1 was not as significant as that of varying the number of turns (n), where the decrement of La is only in the range of 0.1–0.2 µH, which is from 2.82 µH 2.58 µH. Similarly, Designs 2 and 3 show a minimal decrement of La, which is from 1.41 µH to 1.26 µH and 0.57 µH to 0.48 µH, respectively. The Ra values also show a minor decrement for each of the antenna designs, approximately in the range of 0.04–0.21 Ω, due to the reduction of the proximity effect, which is caused by the current induced in the conductors by a magnetic field generated between the neighbouring coil wires [22].

3.3 Different Widths of the Conductor, w

The width of the conductor is represented as the antenna resistance in the antenna equivalent circuit. Following Equation (3), the width of the conductor (w) is inversely proportional to the AC resistance of the conductor (R_{AC}) [21].

$$R_{AC} = \frac{1}{(w + t)} \sqrt{\frac{\pi f \mu}{\sigma}} \tag{3}$$

From the simulation result shown in Figure 4 (b), the antenna resistance and inductance clearly decrease with the increase of the conductor width (w) from 0.7 mm to 0.9 mm given the inversely proportional relationship between them. Design 1 shows a decrement of Ra from 1.61 Ω to 1.43 Ω, followed by Designs 2 and 3, which show a minimal decrement from 0.93 Ω to 0.87 Ω and 0.51 Ω to 0.41 Ω, respectively. By increasing the width of the conductor, the effective area of the current flow is increased, leading to the reduction of the antenna resistance [23]. A similar trend can be seen for the variation of antenna inductance, where a minimal decrement of La is observed in all antenna designs, from 2.73 µH to 2.45 µH for Design 1, 1.36 µH to 1.17 µH for Design 2 and 0.54 µH to 0.43 µH for Design 3.

p-ISSN 1675-7939; e-ISSN 2289-4934

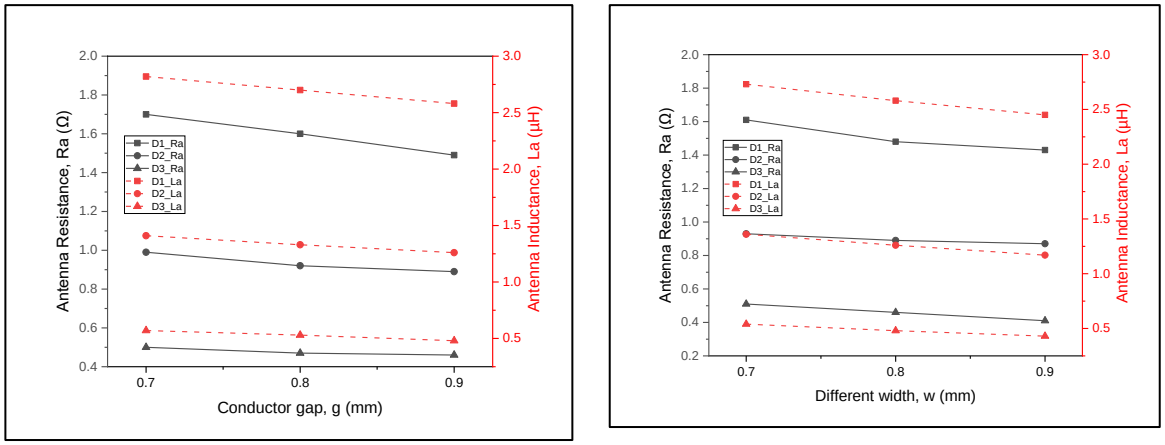

(a) (b)

Figure 4: Ra and La with respect to the (a) conductor gap, g and (b) conductor width, *w*

In conclusion, the larger the surface area of the antenna, the larger will be the antenna inductance and antenna resistance regardless of the shape, (either square or rectangular). Figure 5 summarizes the final value of antenna inductance (La) and resistance (Ra) for all antenna designs. Design 1 shows the highest value of La and Ra due to the large surface area of the antenna, followed by Designs 2 and 3. Since the amount of magnetic field that passes through a given surface (magnetic flux, Φ) is proportional to the antenna inductance, as referred to in Equation (4), the higher the inductance value, the higher will be the induced magnetic field. Accordingly, the tag reading range and power received will also increase. Owing to this outcome, the miniaturization of the tag antenna will have a trade-off in terms of the reading range and power received as a result of the reduced antenna inductance. Therefore, to obtain a high inductance value for the NFC tag antenna, the surface area and number of turns need to be large while the conductor gap and the conductor width need to be small.

$$L=\frac{N\Phi}{I} \tag{4}$$

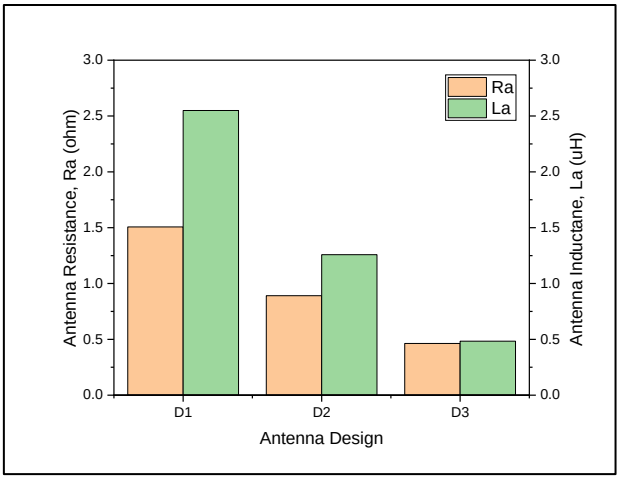

Figure 5: Ra and La for all antenna designs

p-ISSN 1675-7939; e-ISSN 2289-4934

4. RESULT AND DISCUSSION

For the NFC tag antenna to achieve the targeted resonant frequency of 13.56 MHz, the value of tunable capacitance (C_{tun}) needed to be tuned carefully. Using CST Design Studio, the tunable capacitor was tuned until the required resonant frequency of 13.56 MHz was achieved. The simulated tunable capacitance values and inductance value of each antenna design are depicted in Figure 6 (a). Since the antenna inductance is inversely proportional to the capacitance, in reference to Equation (1), the smaller the size of the antenna, the larger the tunable capacitance required. Results illustrate that the smallest tag antenna, Design 3, requires the highest value of tunable capacitance (i.e. 250 pF) due to the smallest value of the antenna inductance. This is followed by Design 2 with 74.5 pF of tunable capacitance and Design 1 with 18.2 pF. The higher the capacitance value, the larger will be the power consumption. Figure 6 (b) shows the S_{11} results for all antenna designs after the tunable capacitor is inserted at the port of the antenna. Each of the antenna designs resonated at 13.56 MHz with different values of reflection coefficient due to the nonlinear resistance of the NFC chip. The reflection coefficient value for the NFC antenna is not necessarily below -10 dB because the antenna does not radiate the power. It works based on the inductive coupling with the reader antenna, which also resonates at the same operating frequency of 13.56 MHz. Therefore, the critical factor for successful communication is ensuring that the tag antenna resonates within the frequency range of the reader antenna to establish the coupling.

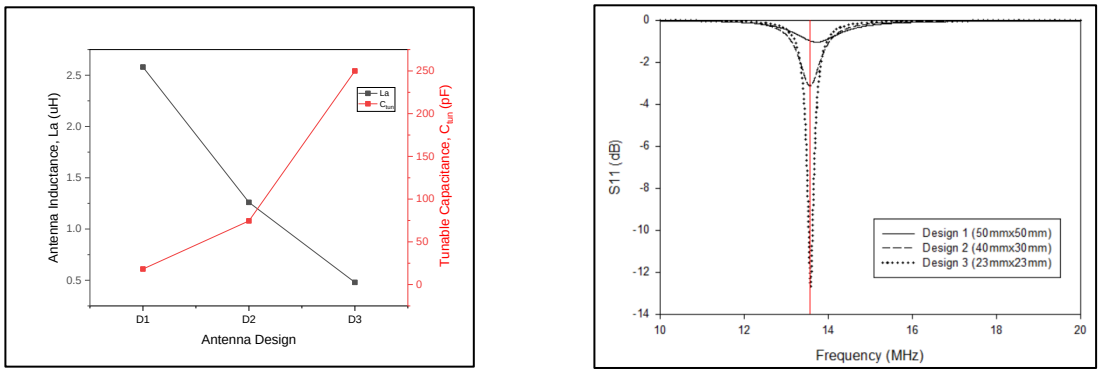

(a) (b)

Figure 6: (a) Antenna inductance and tunable capacitance and (b) S_{11} results for NFC tag antenna

The received voltage for each antenna design is also different depending on the size of the antenna. Using the default NFC reader antenna in the CST Simulation software, the simulation of the reader and the proposed tag antenna as depicted in Figure 7 (a) was carried out to observe the received voltage at the NFC tag antenna. The distance between the reader and the tag was 20 mm. Simulation results seen in Figure 7 (b) show that the Design 1 antenna received the highest voltage compared to other antenna designs with the voltage value of 4.1 V, followed by Design 2 antenna with 3.8 V and Design 3 with 2.6 V. From this result, it can be concluded that the larger the size or the surface area of the antenna, the larger will be the amount of magnetic field induced in the tag antenna, hence the increase in the induced current and voltage received by the tag antenna.

p-ISSN 1675-7939; e-ISSN 2289-4934

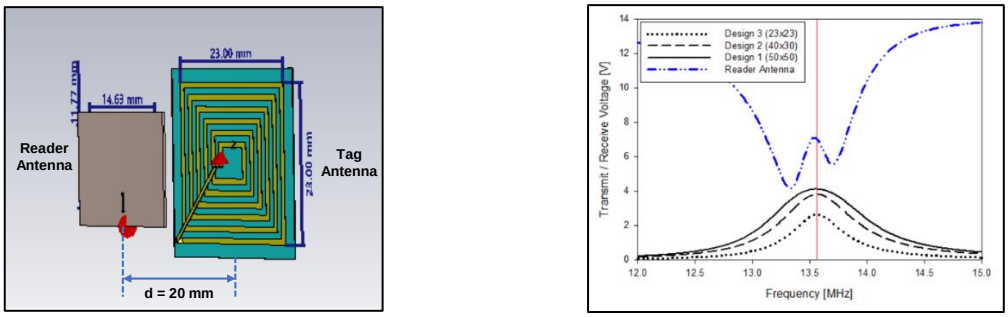

(a) (b)

Figure 7: (a) Reader and Tag (b) transmitted and received voltage of NFC reader and tag antennas, respectively

The flexibility of the antenna designs was then analysed by bending the antenna at different angles through variations of cylindrical bend radius ® as shown in the inset of Figure 8 (a). As the radius of the cylinder increases, the smaller the bending angle becomes. Figures 8 (a)–(c) illustrate the reflection coefficient of all antenna designs with respect to the different bending conditions. From the simulated results, Design 1 shows a significant shift of resonant frequency, with 0.3 and 0.7 MHz when the radius is reduced to 20 and 15 mm, respectively. Design 2 shows a small frequency shift of only 0.23 MHz when the radius is 15 mm. Meanwhile, Design 3 is robust against bending deformation, as the shifting of frequency is nearly indistinguishable. It can be concluded that the smaller the size of the antenna, the more robust will the antenna be in terms of bending. This is because the inductance of the smaller-sized antenna is not affected much by bending deformation compared to that of the larger-sized antenna. For the larger size antenna, the antenna inductance will be decreased with the increase of the bending angle, resulting in the shifting of the resonant frequency to a higher frequency. Figure 9 (d) depicts the relation between the antenna inductance and cylinder bending radius for all antenna designs.

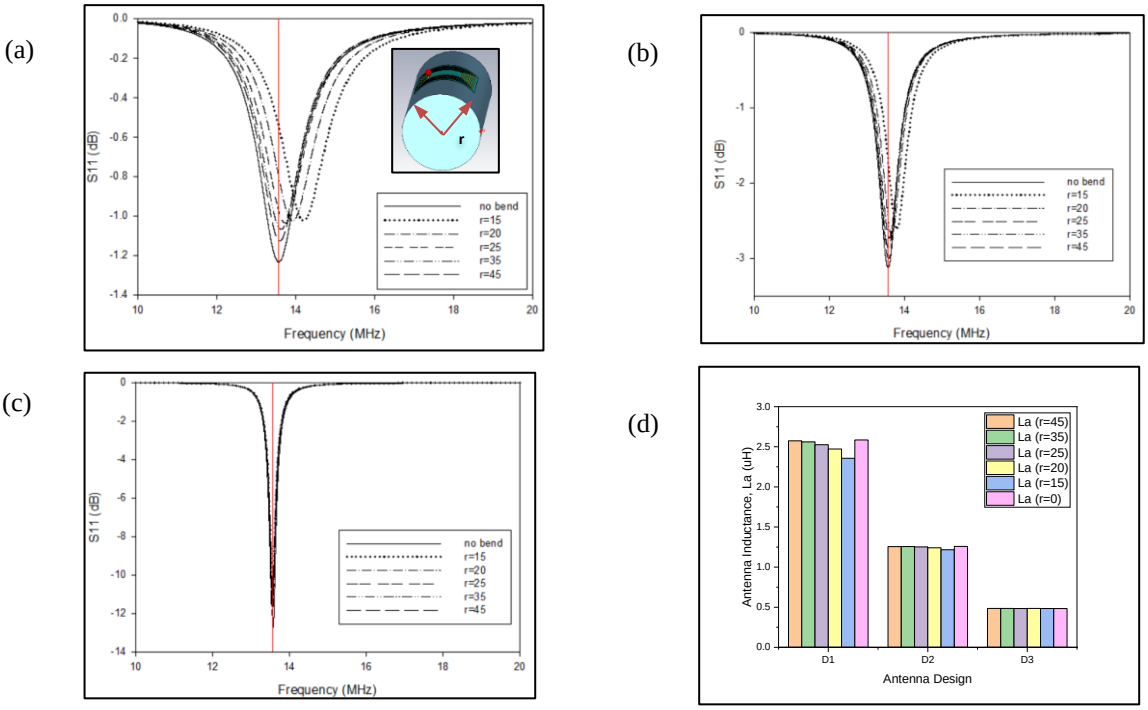

Figure 8: Antenna reflection coefficient with respect to the variation of cylinders radius (r) for (a) Design 1, (b) Design 2 and (c) Design 3 and (d) La with the variation of r for all antenna designs

p-ISSN 1675-7939; e-ISSN 2289-4934

To verify the result experimentally, two of the antenna designs were fabricated, namely Designs 1 and 2, as shown in Figure 9 (a), by using by using a low-cost direct ink writing (DIW) technology. Voltera V-One PCB printer (Figure 9 (b)) was used to fabricate the antenna in the Collaborative Microelectronic Design Excellence Centre. The antenna was printed in three layers. The first layer was the coil, while the second layer was the insulator and the third layer was the bridge, which was used to connect the outer and inner coils of the antenna. The first and third layers were printed using silver nanoparticle ink from Voltera, while the insulator was printed using UV curing solder mask ink from Mechanic.

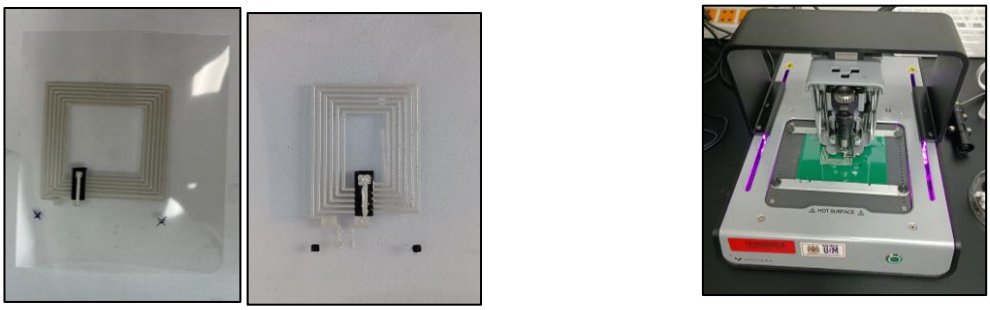

(a) (b)

Figure 9: (a) Prototype of Designs 1 and 2 NFC tag antenna (b) Voltera V-One PCB Printer

Figure 10 (a) shows the measurement of antenna inductance and resistance using HM8118 LCR Bridge from Rohde & Schwarz. The measured values for the Design 1 and Design 2 antennas were compared with those from the simulation and reported in Table 3. The antenna inductance showed only a small deviation between the simulated and measured results, which are 0.31 and 0.03 µH for the Design 1 and Design 2 antennas, respectively. For antenna resistance, however, the measured result showed a large deviation from the simulated results, which are around 27 and 11 Ω difference for the Design 1 and Design 2 antennas, respectively. A few possible factors might have contributed to the high value of the measured antenna resistance including the reduction of the conductivity value for fabricated silver ink as compared to the simulation. This might be due to the curing process conducted after the printing process to harden the material. For verification, the conductivity of the silver printed antenna has been measured using 2-contact probe method as shown in Figure 10 (b). The conductivity value has been calculated using Equation (5), where I and V values were obtained from the 2-contact probe measurement method as shown in Figure 10 (c) , while L, w and t are the sample length, width and thickness respectively. From the calculation, the average value of the conductivity achieved is 2.32 x 10^5 S/m, which are two orders lower than the simulated conductivity value.

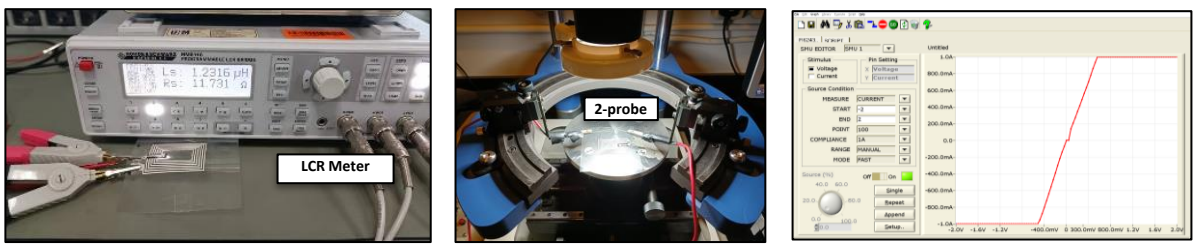

(a) (b) (c)

Figure 10: (a) Measurement of antenna inductance and resistance using HM8118 LCR Meter (b) Measurement of conductivity using 2-contact probe method (c) I-V curve measurement result

p-ISSN 1675-7939; e-ISSN 2289-4934

$$\sigma = \frac{I}{V} \times \frac{L}{wt} \tag{5}$$

Table 3: Antenna Inductance and Resistance for Designs 1 and 2

Parameter	Design 1		Design 2	
	Simulation	Measurement	Simulation	Measurement
Antenna Inductance, La [µH]	2.58	2.89	1.26	1.23
Antenna Resistance, Ra [Ω]	1.49	28.53	0.89	11.73

Figure 11 (a) shows the use of a vector network analyser (VNA) and loop probe to measure the antenna resonance frequency with respect to the tuning capacitance. The antenna was connected parallel to the tuning capacitance C_{tun} on the breadboard and the RF430FRL152HEVM board from Texas Instrument, which consists of an internal capacitance C_{int} of 35 pF. An NFC-enabled smartphone, Xiaomi 11, was also used to detect the tag and measure the tag reading range. Figures 11 (b) (i) and (ii) depict respectively the plots of the Designs 1 and 2 antenna resonance frequency together with the tag reading range with respect to the tuning capacitance values from 0 pF until 200 pF. The maximum distance that the reader can detect the Design 1 tag antenna is 3 cm with the tuning capacitance values in the range of 5 – 20 pF. Meanwhile, for Design 2, the maximum distance that the reader can detect the tag is 2 cm with the tuning capacitance values in the range of 60 – 75 pF. This finding coincides with the simulated result that required 18 pF as tuning capacitor for Design 1 and 75 pF for Design 2. However, the resonant frequency for maximum distance is slightly shifted to the higher frequency, which is around 18 and 15–17 MHz for the Design 1 and Design 2 antennas, respectively. The shifting of the resonant frequency is expected because an external cable is used to connect the antenna to the capacitors and the board, which will increase the resistance and contribute to the shifting of the resonant frequency to the higher frequency. Directly connecting the SMD capacitor and the chip to the antenna will reduce the resistance and shift the frequency back to the required operating frequency.

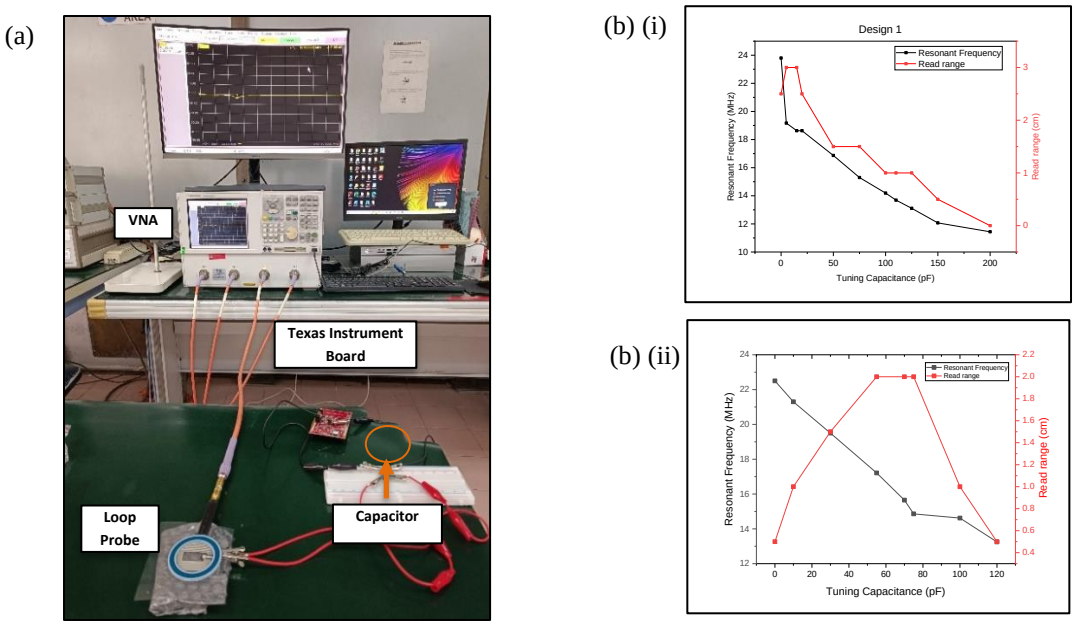

Figure 11: (a) Measurement of antenna resonance frequency using VNA (b) Measured result of antenna resonance frequency and tag reading range with respect to the C_{tun} for (i) Design 1 and (ii) Design 2

p-ISSN 1675-7939; e-ISSN 2289-4934

Figure 12 (a) shows the measurement of output voltage with respect to the distance between NFC tag and NFC reader, which was a Xiaomi 11 smartphone. The tag antenna was connected to an oscilloscope while the NFC reader was placed a few distance on top of the tag antenna, where a stable, height-adjustable platform was employed to vary the distance between the antenna and the reader. The distance (d) between the reader and the tag antenna was varied from 0 to 10 cm with 1 cm intervals, and the output voltages from the Design 1 and Design 2 antennas were recorded and plotted in a graph shown in Figure 12 (b). Following the results depicted in Figure 13, output voltage is decreased with the increase of the distance between the reader and the tag antenna for both antenna designs. This is due to the reduction of mutual inductance between the coil antennas with respect to the distance. The maximum values of the output voltage are 1.8 V for Design 1 and 1.6 V for Design 2, when the reader and the tag antenna are 0 cm from each other. When the output voltage is lower than 0.3 V, the tag antenna cannot be detected anymore. In comparison to the simulation, the measured output voltage is lower due to a few factors, including different reader antenna performance between the simulation and measurement and the existence of parasitic elements from the external cable connections.

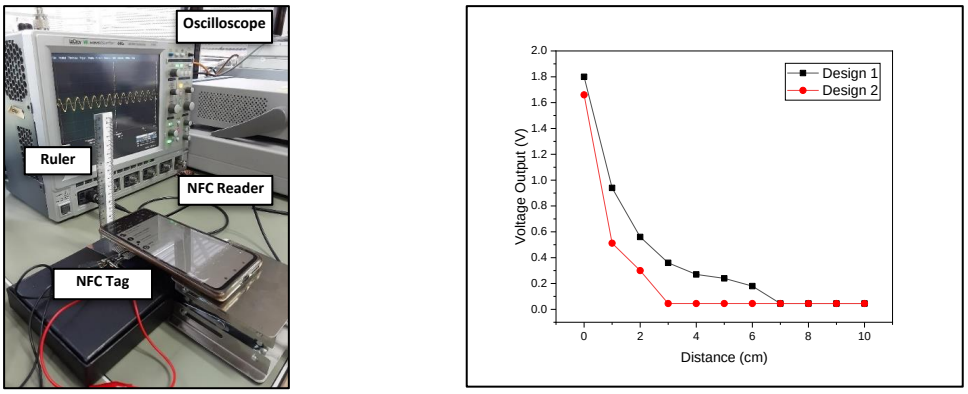

(a) (b)

Figure 12: (a) Measurement setup of output voltage and (b) measured output voltage with respect to the distance

The bending effect was also observed for the Design 2 antenna, which is the medium-sized design between Designs 1 and 3. The tag antenna was attached to different sizes of cylinder foam, as depicted in Figure 13. The tag reading range was measured and the antenna resonant frequency with a fixed value of tuning capacitor (i.e., 75 pF) was observed.

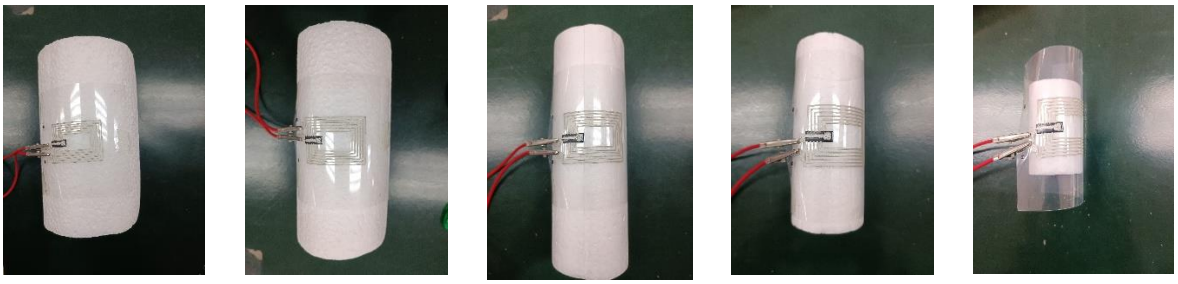

(a) (b) (c) (d) (e)

Figure 13: Design 2 antenna attached on cylinder foams with different radius: (a) 4.5 cm, (b) 3.5cm, (c) 2.5 cm, (d) 2 cm and (e) 1.5 cm

p-ISSN 1675-7939; e-ISSN 2289-4934

From the measurement, it is observed that the antenna resonant frequency remains almost the same for different sizes of cylinder foams, as depicted in Figure 14 (a), which agrees well with the simulated result. However, the tag reading range is decreased with the reduced cylinder radius, as illustrated in Figure 14 (b). This is because the bending angle is increased when the radius of the cylinder is reduced, and so the surface area of the antenna, which is exposed to the reader, is decreased. Since the surface area is proportional to the induced magnetic field, the decrease of the antenna surface area will reduce the amount of magnetic field induced in the tag antenna, which contributes to the reduction of the tag reading range. With the reduction of the cylinder radius from 4.5 cm to 1.5 cm, the tag reading range is reduced from 2 cm to 0.5 cm.

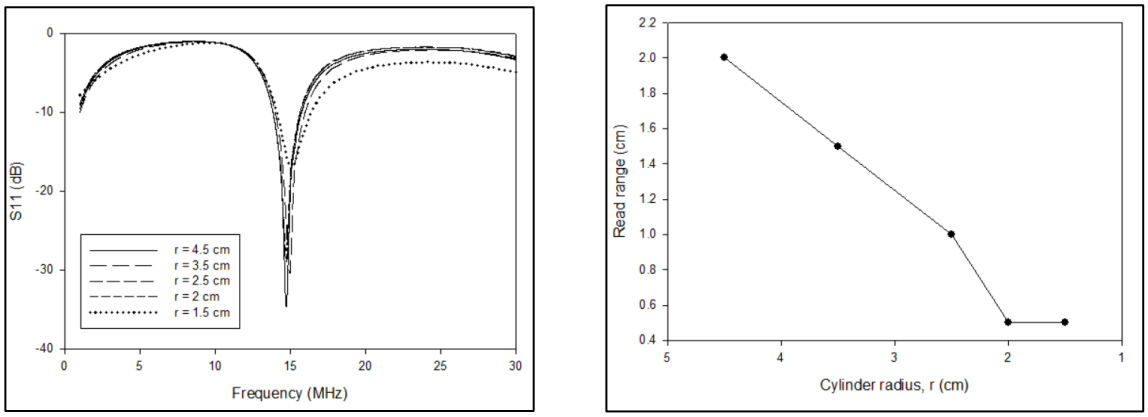

(a) (b)

Figure 14: (a) Antenna resonant frequency with respect to the cylinder radius. (b) The tag reading range with respect to the cylinder radius

5. CONCLUSION

The analysis of three sizes of NFC tag coil antenna was effectively demonstrated through simulation and measurement. The different sizes of the tag antenna contributed to different characteristics in terms of the electrical properties, bending effect, antenna matching and reading range. A parametric study was also conducted to determine the effect of varying the antenna parameters, including the size, number of turns, gap between the conductors and conductor width, to the antenna's electrical parameters, such as inductance and resistance. The smaller the antenna size and the number of turns, the lower will be the inductance value, which will reduce the induced magnetic field and hence lower the reading range. However, the smaller size of the tag antenna is more flexible on different surface structures because the shifting of the antenna resonant frequency is nearly indistinguishable with different bending angles. Two antenna designs, Design 1 and Design 2, were fabricated and their antenna inductance, resistance, tuning capacitance, reading range and output voltage were observed. The measured antenna inductance and tuning capacitance greatly coincide with the simulation. However, the antenna resistance and output voltage show some deviations from the simulated result due to minor factors in fabrication and measurement processes. The flexibility of the fabricated Design 2 antenna was also observed and evaluated. The antenna resonant frequency only shows a small deviation when the bending angle is increased, but the reading range is reduced with the increase of the bending angle. For future related studies, all possible errors identified during the measurement will be investigated and improved when measuring other tag antenna designs to

p-ISSN 1675-7939; e-ISSN 2289-4934

achieve more accurate results. The presented characteristics will be a guide to designing and fabricating better NFC tag antennas for different applications.

ACKNOWLEDGEMENT

The author would like to convey their deepest gratitude to the Antenna and Microwave Research Group (AMRG), the Antenna Research Center, the Collaborative Microelectronic Design Excellence Centre USM and Universiti Teknologi Mara Cawangan Pulau Pinang for their support and guidance.

CONFLICT OF INTEREST

The authors declare that there is no conflict of interest regarding the publication of this paper.

REFERENCES

[1] S. Kolev, "Designing a NFC system," in *2021 56th International Scientific Conference on Information, Communication and Energy Systems and Technologies, ICEST 2021 - Proceedings*, 2021, pp. 111–113. doi: 10.1109/ICEST52640.2021.9483482.

[2] A. Lazaro, R. Villarino, and D. Girbau, "A survey of NFC sensors based on energy harvesting for IoT applications," *Sensors (Switzerland)*, vol. 18, no. 11, 2018, doi: 10.3390/s18113746.

[3] B. B. Maskey *et al.*, "A Smart Food Label Utilizing Roll-to-Roll Gravure Printed NFC Antenna and Thermistor to Replace Existing 'Use-By' Date System," *IEEE Sens J*, vol. 20, no. 4, pp. 2106–2116, 2020, doi: 10.1109/JSEN.2019.2948752.

[4] H. Witschnig, E. Sonnleitner, J. Bruckbauer, and E. Merlin, "Eigenvalue Analysis of Close Coupled 13 . 56 MHz RFID-Labels," *IEEE Microwave Symposium Digest*, pp. 324–327, 2006.

[5] Z. Cao *et al.*, "Near-field communication sensors," *Sensors (Switzerland)*, vol. 19, no. 18, 2019, doi: 10.3390/s19183947.

[6] J. I. Cairó, J. Bonache, and F. Paredes, "Reconfigurable System for Wireless Power Transfer (WPT) and Near Field," *IEEE Journal of Radio Frequency Identification*, vol. 1, no. 4, pp. 253–259, 2018.

[7] M. H. Misran and S. K. A. Rahim, "Optimum transmitter receiver ratio for maximum wireless energy transfer," *Indonesian Journal of Electrical Engineering and Computer Science*, vol. 5, no. 3, pp. 599–605, 2017, doi: 10.11591/ijeecs.v5.i3.pp599-605.

[8] X. Sun *et al.*, "Wearable Near-Field Communication Sensors for Healthcare : Materials , Fabrication and Application," *Micromachines (Basel)*, 2022.

[9] J. Kim *et al.*, "Miniaturized Flexible Electronic Systems with Wireless Power and Near-Field Communication Capabilities," *Adv Funct Mater*, pp. 4761–4767, 2015, doi: 10.1002/adfm.201501590.

[10] A. Scidà *et al.*, "Application of graphene-based flexible antennas in consumer electronic devices," *Materials Today*, vol. 21, no. 3, pp. 223–230, 2018, doi: 10.1016/j.mattod.2018.01.007.

[11] T. B. Nguyen, T. H. Nguyen, and W. Y. Chung, "Battery-free and noninvasive estimation of food ph and co2 concentration for food monitoring based on pressure measurement," *Sensors (Switzerland)*, vol. 20, no. 20, pp. 1–12, 2020, doi: 10.3390/s20205853.

[12] A. Lazaro, M. Boada, R. Villarino, and D. Girbau, "Color measurement and analysis of fruit with a battery-less NFC sensor," *Sensors (Switzerland)*, vol. 19, no. 7, 2019, doi: 10.3390/s19071741.

[13] M. Benavides, D. Miralles, A. Andújar, and J. Anguera, "Effects on human body and conductive body over a near field communication antenna," *J Electromagn Waves Appl*, vol. 35, no. 9, pp. 1235–1246, 2021, doi: 10.1080/09205071.2021.1875889.

p-ISSN 1675-7939; e-ISSN 2289-4934

[14] Y. Z. N. Htwe and M. Mariatti, "Printed graphene and hybrid conductive inks for flexible, stretchable, and wearable electronics: Progress, oppotunities, and challenges," Journal of *Science: Advanced Materials and Devices*, vol. 7, no. 2, p. 100435, 2022, doi: 10.1016/j.jsamd.2022.100435

[15] X. Zhang, X. Shan, and J. Wei, "Hybrid flexible smart temperature tag with NFC technology for smart packaging," *2017 IEEE 19th Electronics Packaging Technology Conference, EPTC 2017*, vol. 2018-Febru, pp. 1–5, 2018, doi: 10.1109/EPTC.2017.8277578.

[16] T. Leng *et al.*, "Printed graphene/WS2 battery-free wireless photosensor on papers," *2d Mater*, vol. 7, no. 2, 2020, doi: 10.1088/2053-1583/ab602f.

[17] I. Ortego, N. Sanchez, J. Garcia, F. Casado, D. Valderas, and J. I. Sancho, "Inkjet printed planar coil antenna analysis for NFC technology applications," *Int J Antennas Propag*, vol. 2012, 2012, doi: 10.1155/2012/486565.

[18] Y. Jiang, K. Pan, T. Leng, and Z. Hu, "Smart Textile Integrated Wireless Powered near Field Communication Body Temperature and Sweat Sensing System," *IEEE J Electromagn RF Microw Med Biol*, vol. 4, no. 3, pp. 164–170, 2020, doi: 10.1109/JERM.2019.2929676.

[19] Texas Instruments, "RF430FRL15xH NFC ISO 15693 Sensor Transponder," 2014.

[20] K. Saito, T. Nakamura, K. Kamezawa, R. Ikeda, Y. Hashimoto, and B. Shizuki, "Japanese patterns as NFC antennas for interactive urushi-ware," *TEI 2020 - Proceedings of the 14th International Conference on Tangible, Embedded, and Embodied Interaction*, no. February 2020, pp. 443–451, 2020, doi: 10.1145/3374920.3374952.

[21] Microchip, "Antenna Circuit Design for RFID Applications," 2003. [Online]. Available: http://ww1.microchip.com/downloads/en/AppNotes/00710c.pdf

[22] B. Lee, B. Kim, F. J. Harackiewicz, S. Member, B. Mun, and H. Lee, "NFC Antenna Design for Low-Permeability Ferromagnetic Material," *IEEE Antennas Wirel Propag Lett*, vol. 13, pp. 59–62, 2014.

[23] Y. J. Park, J. E. Kim, S. H. Lee, and K. H. Cho, "An Effective Design Formula for Single-Layer Printed Spiral Coils with the Maximum Quality Factor (Q-Factor) in the Megahertz Frequency Range," *Sensors (Basel)*, vol. 22, no. 20, 2022, doi: 10.3390/s22207761.

p-ISSN 1675-7939; e-ISSN 2289-4934